TABLE IV. g values and the wave functions of NpO_2^{+2} in the crystal field of sixfold symmetry reported by Eisenstein and Pryce (Ref. 4).

Electronic state Axial	C_{3i}	Energy (cm^{-1})	$g_{\parallel}$	$\lvert g_{\perp}\rvert$	Wave function
$\lvert -3+\rangle$	$\mu=\pm\frac{1}{2}$	0	−4.2	0.17	$0.8975\lvert -3+\rangle-0.4246\lvert -2-\rangle-0.1134\lvert +3+\rangle$
$\lvert +2-\rangle$	$\mu=\pm\frac{3}{2}$	664	2.1	0	$0.9855\lvert +2-\rangle-0.1708\lvert +1+\rangle$
$\lvert -2-\rangle$	$\mu=\pm\frac{1}{2}$	6752	−4.3	1.84	$0.8707\lvert -2-\rangle+0.3729\lvert -3+\rangle-0.3207\lvert +3+\rangle$
$\lvert +3+\rangle$	$\mu=\pm\frac{1}{2}$	8168	6.5	2.01	$0.9407\lvert +3+\rangle+0.2349\lvert -3+\rangle 0.2446\lvert -2-\rangle$
$\lvert +1-\rangle$	$\mu=\pm\frac{1}{2}$	18 100	0.0	0.43	$0.9981\lvert +1-\rangle-0.0627\lvert 0+\rangle$
$\lvert +1+\rangle$	$\mu=\pm\frac{3}{2}$	21 100	3.9	0.0	$0.9855\lvert +1+\rangle+0.1708\lvert +2-\rangle$
$\lvert 0+\rangle$	$\mu=\pm\frac{1}{2}$	79 760	2.0	2.43	$0.9981\lvert 0+\rangle+0.0627\lvert +1-\rangle$

E_5, and E_9 showed no Zeeman effect when the magnetic field of 26 kG was parallel to the c axis. The $g_{\parallel}$ values of these levels were interpreted as the same as that of the ground state. The authors are uncertain that this is the case. However, this seems to be the only solution until further information is obtained in the future.

PHYSICAL REVIEW VOLUME 187, NUMBER 2 10 NOVEMBER 1969

Optical Absorption of Fe^{2+} in CdTe in the Near and Far Infrared

GLEN A. SLACK, S. ROBERTS, AND J. T. VALLIN
General Electric Research and Development Center, Schenectady, New York 12301
(Received 11 June 1969)

The optical-absorption spectrum of Fe^{2+} $3d^6$ impurities in CdTe crystals has been measured over the wave-number range from 10 to 120 cm^{-1} in the far infrared at 4.2 and 20°K, and from 2000 to 13 000 cm^{-1} in the near infrared at 2, 14, and 300°K. Transitions between the five spin-orbit levels of the ^5E ground state have been seen in the far infrared, while transitions from ^5E to the $^5T_2$ and possibly higher states have been seen in the near infrared. The far-infrared results give the energies for two of the ^5E levels as $\Gamma_1=0$ and $\Gamma_4=18.6$ cm^{-1}, and two unspecified lines at $\bar{\nu}=66.7$ and 73.2 cm^{-1}. These results also give phonon energies at several critical points in the Brillouin zone as $TA(L)=36$ cm^{-1}, $TA(X)=46$ cm^{-1}, $LA(L)=104.5$ cm^{-1}. The Γ_4 level of ^5E has been found to split in a magnetic field with $g=1.02$. The magnetic susceptibility of Fe^{2+}-doped CdTe has been measured from 4 to 300°K, and the results agree with predictions based on the calculated level positions of the ^5E state in an applied magnetic field. An appendix is presented in which the theory of the splitting of the ^5D free-ion state in the tetrahedral crystal field is given, and the resultant energies and wave functions of the individual spin-orbit levels are tabulated.

INTRODUCTION

WHEN Fe^{2+} impurities are substitutionally incorporated for Cd in the cubic crystal CdTe the ^5D free ion state of the $3d^6$ electrons splits into two orbital states, ^5E and $^5T_2$. In the tetrahedral crystal field symmetry T_d, the ^5E state is lower in energy than the $^5T_2$. Many of these crystal field calculations have been done, though somewhat incorrectly, by Low and Weger.[1] First-order and second-order spin-orbit interactions split these 10- and 15-fold degenerate states even further. The resultant ground level is a Γ_1 singlet. Optical transitions from this singlet to other levels of ^5E can be seen in the far-infrared spectral region for wave numbers $10<\bar{\nu}<120$ cm^{-1}. Transitions from Γ_1 to levels of the $^5T_2$ state can be seen in the near infrared for $2500<\bar{\nu}<4000$ cm^{-1}. Similar far-infrared studies on Fe^{2+} impurities in cubic ZnS have been reported by Slack, Roberts, and Ham,[2] which will be referred to hereafter as SRH. Studies in the near infrared have been reported by Slack, Ham, and Chrenko,[3] or SHC, for Fe^{2+} in CdTe, ZnS and $MgAl_2O_4$. The present studies thus report the far-infrared results on Fe^{2+} in CdTe for the first time, and extend the previous near-infrared measurements.

In addition to these measurements in zero magnetic field the splitting of the optical-absorption line at $\bar{\nu}=18.6$ cm^{-1} has been measured in magnetic flux densities[4] up to 1.6 T (1.6×10^4 G). This measurement

[1] W. Low and M. Weger, Phys. Rev. **118**, 1119 (1960); **120**, 227(E) (1960).

[2] G. A. Slack, S. Roberts, and F. S. Ham, Phys. Rev. **155**, 170 (1967).

[3] G. A. Slack, F. S. Ham, and R. M. Chrenko, Phys. Rev. **152**, 376 (1966).

[4] We have adopted the International System of units (SI) in this paper. See U. S. Natl. Bur. Std. Tech. News Bull. **48**, 61 (1964); P. H. Bigg, Brit. J. Appl. Phys. **15**, 1243 (1964); also J. A. Stratton, *Electromagnetic Theory* (McGraw-Hill Book Co., New York, 1941).

allows us to determine the g factor for the Γ_4 triplet level, and to compare it with theory. As a further check, we have measured the magnetic susceptibility χ of Fe^{2+}-doped CdTe versus temperature in order to further verify the energy-level structure of the ^5E state. There are no previous measurements on the g value of tetrahedral Fe^{2+}, and only a few previous measurements of the χ of undoped CdTe are available in the literature.[5]

SAMPLES

The samples of CdTe and (Mg-Cd)Te used in these experiments were all grown in this laboratory from the melt using a restricted molten-zone technique[6] (see Acknowledgments). The starting materials were high purity Cd,[7] Te,[8] and moderate purity Mg.[9] The Fe was incorporated during the growth using high purity Fe[10] and some excess Te. The samples were cut in the shape of circular discs and the faces were polished for the optical measurements. The far-infrared samples were approximately 1.2 cm in diameter and 0.3 cm thick. The near-infrared samples were about 0.5 cm in diameter and 0.1 cm thick. The optical-absorption coefficient α was determined from percent transmission[2,3] measurements.

One of the problems encountered in this study was the determination of the Fe^{2+} content of the CdTe crystals. Standard wet chemical analyses give the total Fe concentration, which includes any precipitated Fe. In order to establish some solubility limits for Fe, a number of Fe-doped CdTe samples were annealed at 1073°K (800°C) for a period of 14 h under various partial pressures of Cd. The samples were placed in small vitreous SiO_2 capsules to which a weighed amount of Cd (or Te) was added before sealing the capsule. The Fe^{2+} concentration was thus equilibrated at 1073°K, and the results showed that the higher the Cd pressure the lower the resultant Fe^{2+} concentration. The results for two different series of CdTe crystals are shown in Fig. 1. The equilibrium Fe^{2+} concentration for the maximum Cd pressure at 1073°K is $\sim 2\times10^{18}$ atoms/cm^3, whereas it is 4×10^{19} atoms/cm^3 for the minimum Cd (maximum Te) pressure. The relationship of the Te and Cd pressures in equilibrium with CdTe at 1073°K has been given by previous authors.[11–13] The specification of the partial pressure of Cd and the temperature, as in Fig. 1, fixes the partial pressure of Te. Thus at 1073°K, the Fe^{2+} solubility varies by a factor of 20, depending on the ambient atmosphere. The Fe^{2+} content was determined from optical-absorption measurements. The higher of the two curves in Fig. 1 was measured for samples which had a total Fe concentration of about 3.5×10^{19} Fe/cm^3. The lower curve in Fig. 1 was determined for samples which had a total Fe concentration of only 3.5×10^{18} atoms/cm^3. All of the Fe will occur as Fe^{2+} if these latter samples are annealed under conditions such that the Cd pressure <10 torr. One sample was then annealed at a Cd pressure of 1 torr and was used as a standard to determine the optical-absorption coefficient α per unit Fe concentration. At 300°K the α at the peak at the Fe^{2+} absorption band at wave-number $\bar{\nu}=2750$ cm^{-1} is $\alpha(\text{peak})=1.7$ cm^{-1} for 10^{18}/cm^3 of Fe^{2+}. This number was used in determining the Fe^{2+} concentration in all the other crystals. This particular calibration scheme was not used in SHC, and hence the absorption values per Fe^{2+} ion tend to be lower by about a factor of 2 than those used here. The previous assumption was that all of the Fe in the as-grown crystal occurred as Fe^{2+}, but this assumption has been found to be false for most CdTe crystals. The disposition of the rest of the Fe is unknown.

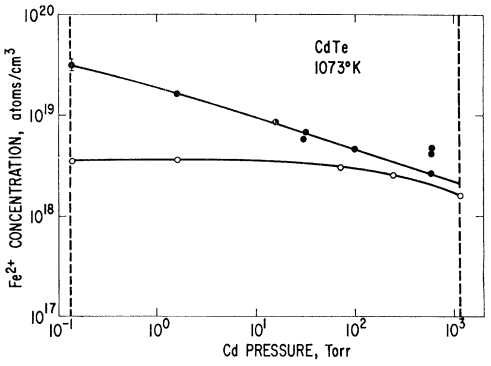

FIG. 1. Fe^{2+} concentration in CdTe at equilibrium at an annealing temperature of 1073°K as a function of the partial pressure of cadmium vapor. Results for two different samples with total iron concentrations of 3.5×10^{18} (lower curve) and about 4×10^{19} (upper curve) iron atoms/cm^3 are shown.

APPARATUS

The far-infrared measurements for $10<\bar{\nu}<200$ cm^{-1} were made with a diffraction-grating spectrometer previously described.[14] The near-infrared measurements at 300°K for $2000<\bar{\nu}<14\,000$ cm^{-1} were made with a Beckman[15] IR7 and a Cary[16] Model 14 spectrometer. The lower-temperature data from 77 to 2°K for $2000<\bar{\nu}<4000$ cm^{-1} were taken with a Spex[17] 1700 Czerny-Turner spectrometer. The sample was mounted in vacuum in a metal Dewar which employed synthetic sapphire windows. The low-temperature data for 4000

[5] I. V. Potikevich, Ukrainskyu Fiz. Zh. **8**, 793, 1274 (1963); also V. M. Glazov and S. N. Chizhevskaya, Fiz. Tverd. Tela **6**, 1648 (1964) [English transl.: Soviet Phys.—Solid State **6**, 1322 (1964).

[6] M. R. Lorenz and R. E. Halsted, J. Electrochem. Soc. **110**, 343 (1963).

[7] Cominco American Inc., Spokane, Wash.

[8] American Smelting and Refining Co., New York, N. Y.

[9] Dow Chemical Company, Midland, Mich.

[10] Materials Research Corporation, Orangeburg, N. Y.

[11] R. F. Brebrick and A. J. Strauss, J. Phys. Chem. Solids **25**, 1441 (1964).

[12] M. R. Lorenz, J. Phys. Chem. Solids **23**, 1449 (1962).

[13] D. deNobel, Philips Res. Rept. **14**, 430 (1959).

[14] S. Roberts and D. D. Coon, J. Opt. Soc. Am. **52**, 1023 (1962).

[15] Beckman Instruments Inc., Fullerton, Calif.

[16] Applied Physics Corporation, Monrovia, Calif.

[17] Spex Industries Inc., Metuchen, N. J.

$<\bar{\nu}<14\,000$ cm^{-1} were taken with a Cary Model 14 spectrometer. In this region the sample was immersed directly in liquid nitrogen or helium in a glass Dewar which used fused quartz windows.

The magnetic field for the far-infrared measurements was supplied by a small superconducting magnet of Nb-Zr wire operating at dc currents up to 14 A. The magnetic field calibration is accurate to $\pm 2\%$. The magnetic susceptibility measurements were made with a Princeton[18] Model FM-1 Vibrating Sample Magnetometer using magnetic inductions up to 2 T.

RESULTS

Far-Infrared Optical Absorption

The far-infrared optical absorption of pure, undoped CdTe at 4.2 and 20°K is shown in Figs. 2 and 3 for

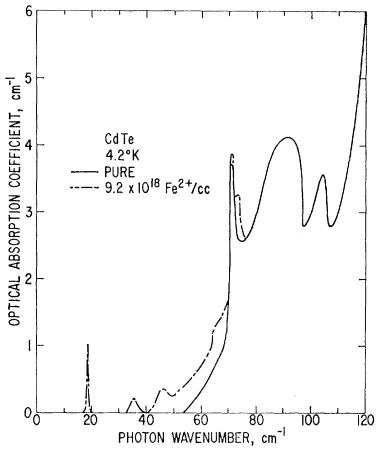

FIG. 2. Optical-absorption coefficient versus photon wave number at a temperature of 4.2°K for both pure and iron doped CdTe. The resolution is about 0.5 cm^{-1}.

$0<\bar{\nu}<120$ cm^{-1}. Notice that the pure CdTe shows no absorption for $0<\bar{\nu}<55$ cm^{-1} but there are some weak bands for $55<\bar{\nu}<120$ cm^{-1}. Some of these weak intrinsic absorption bands have been reported in the literature,[19,20] particularly those at $\bar{\nu}$ of 71 and 114 cm^{-1}. In Figs. 2 and 3 there are absorption bands at $\bar{\nu}$ of 71.3, 92, and 104.5 cm^{-1} that are nearly temperature-independent. The band at 114 cm^{-1} shown in Fig. 3 only appears at $T\geq 20$°K.

When Fe^{2+} impurities are added to the crystal they substitutionally occupy Cd sites, and give rise to further absorption bands in the $0<\bar{\nu}<120$ cm^{-1} region. Some of these bands may be electronic transistions associated with the d-shell levels of the Fe^{2+} ion,[2,3] and some may be lattice bands of CdTe whose absorption is enhanced

[18] Princeton Applied Research, Princeton, N. J.

[19] C. L. Bottger and A. L. Geddes, J. Chem. Phys. **47**, 4858 (1967).

[20] O. M. Stafsudd, F. A. Haak, and K. Radisavljevic, J. Opt. Soc. Am. **57**, 1475 (1967); A. Manabe, A. Mitsuishi, H. Yoshinaga, Y. Ueda, and H. Sei, Technol. Rept. Osaka Univ. **17**, 263 (1967).

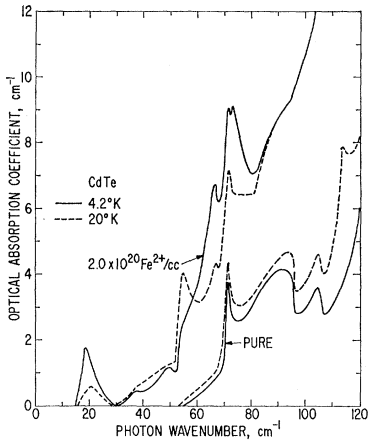

FIG. 3. Optical-absorption coefficient versus photon wave number at 4.2 and 20°K for both pure and iron-doped CdTe. Note that at this high iron concentration the doped crystal has a noticeably higher absorption than the pure one over the whole wave number range. The resolution is about 0.5 cm^{-1}.

by the presence of the Fe impurities. In ZnS doped with Fe^{2+} only the electronic transitions were observed.[2] For CdTe both effects are seen. The electronic transitions are believed to be the absorption peaks at $\bar{\nu}=18.6$, 54.8, 66.7, and 73.2 cm^{-1}, while those at $\bar{\nu}$ of 36, 46, 71.3, 92, 104.5, and 114 cm^{-1} are lattice bands. The reasons for these assignments will be presented later.

The absorption peak at $\bar{\nu}=18.6$ cm^{-1} occurs in Figs. 2 and 3 for both Fe^{2+}-doped crystals. Note, however, that the height of the absorption peak does not increase linearly with the Fe^{2+} concentration. The increasing concentration serves mostly to broaden the absorption band. The bandwidth at half the maximum absorption coefficient is $w=0.5$ cm^{-1} for 9.2×10^{18} Fe^{2+}/cm^3 in Fig. 2 while it is $w=5$ cm^{-1} for 2.0×10^{20} Fe^{2+}/cm^3 in Fig. 3. The integrated absorption A, where

$$A=\int\alpha(\bar{\nu})d\bar{\nu}, \tag{1}$$

is nearly proportional to the Fe^{2+} concentration. This absorption band, which is assigned to be the $(\Gamma_1-\Gamma_4)$ transition[2] of Fe^{2+} is found to split when a magnetic field is applied to the sample. These measurements were made only on the lower Fe^{2+} concentration sample where the band was sufficiently narrow so that the splitting could be observed. The unsplit band at $\bar{H}=0$ occurs at $\bar{\nu}=18.64\pm0.02$ cm^{-1}. The light beam was unpolarized and the magnetic field was applied in two different directions, see Figs. 4(a) and 4(b). The crystallographic orientation of the cubic CdTe sample is, to a first approximation, unimportant, and was not determined. The splitting of the absorption band is shown in Figs. 5(a) and 5(b) for magnetic inductions of 0.0, 0.8, 1.6, and 2.4 T. The band splits into two or three parts depending on the orientation of the magnetic field with respect to the direction of the light beam. Let $\bar{\nu}_h$ be

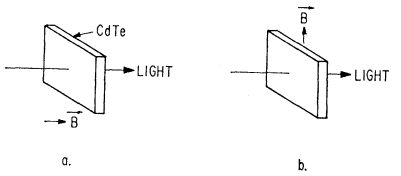

FIG. 4. Two different geometries used for studying the magnetic field effects on the optical absorption of the $\bar{\nu}=18.6$ cm^{-1} line in the far infrared. The longitudinal arrangement is **a**, while the transverse arrangement is **b**. The arrow labeled **B** shows the direction of the applied magnetic field.

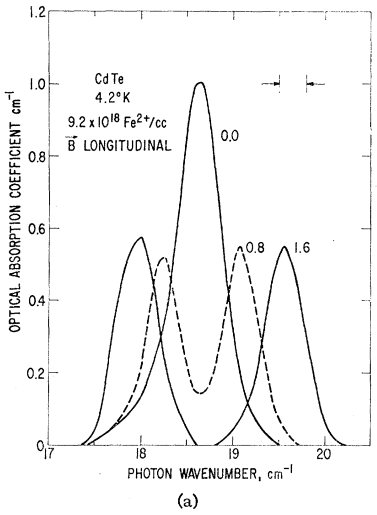

FIG. 5. (a) Optical-absorption coefficient versus photon wave number for the $\bar{\nu}=18.6$-cm^{-1} line at 4.2°K for three different magnetic fields in the longitudinal arrangement [see Fig. 4(a)]. The numbers at the side of each curve give the magnetic induction in T. The resolution is indicated by the arrows. (b) Optical-absorption coefficient versus photon wave number for the $\bar{\nu}=18.6$-cm^{-1} line at 4.2°K for four different magnetic fields in the transverse arrangement [see Fig. 4(b)]. The numbers at the side of each curve give the magnetic induction in teslas. The resolution is indicated by the arrows.

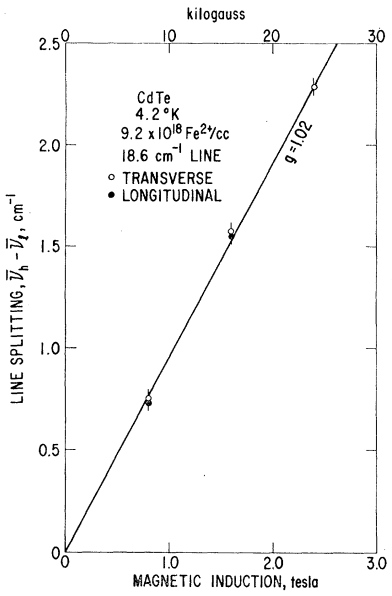

FIG. 6. Over-all splitting, $\bar{\nu}_h-\bar{\nu}_l$, of the 18.6-cm^{-1} line of Fe^{2+} in CdTe at 4.2°K as a function of the magnetic induction. Results for both longitudinal and transverse fields are shown. The derived value of $g=1.02\pm0.03$, corresponding to the straight line.

the wave number of the high-energy peak, $\bar{\nu}_c$ be the center peak [only in Fig. 5(b)], and $\bar{\nu}_l$ be the low-wave-number peak. The difference $\bar{\nu}_h-\bar{\nu}_l$ is found to increase linearly with the magnetic induction, B. This result is shown in Fig. 6. The values of $\bar{\nu}_h$, $\bar{\nu}_c$, $\bar{\nu}_l$ are given in Table I.

Near-Infrared Optical Absorption

The near-infrared optical absorption of pure and Fe^{2+}-doped CdTe has been studied previously[3,21] for the range $1000<\bar{\nu}<13\,000$ cm^{-1}. The Fe^{2+} impurities were found[3] to produce a broad, strong absorption band near $\bar{\nu}=2500$ cm^{-1} that is believed to be caused by the ^5E to $^5T_2$ transition from the ^5E ground state.

TABLE I. Splitting of the $\bar{\nu}=18.6$ cm^{-1} line in a magnetic field at 4.2°K.

B (T)	Line wave number, cm^{-1} [a] $\bar{\nu}_l$	$\bar{\nu}_c$	$\bar{\nu}_h$	$\frac{1}{2}(\bar{\nu}_h+\bar{\nu}_l)$	Difference (cm^{-1}) $(\bar{\nu}_h-\bar{\nu}_l)$	$\vec{B}$ Field Orientation
0.0		18.64		18.64	0.0	Longitudinal
0.8	18.25		19.08	18.67	0.73	
1.6	18.00		19.55	18.78	1.55	
0.0		18.64		18.64	0.0	Transverse
0.8	18.32	18.75	19.1	18.70	0.75	
1.6	18.01	18.83	19.58	18.80	1.57	
2.4	17.88	19.13	20.18	19.02	2.28	
±2%		±0.02 cm^{-1}			±0.04 cm^{-1}	

[a] The subscripts on $\bar{\nu}$, i.e., l, c, and h refer to the lower, center, and higher component of the absorption band.

[21] D. T. F. Marple, Phys. Rev. **150**, 728 (1966).

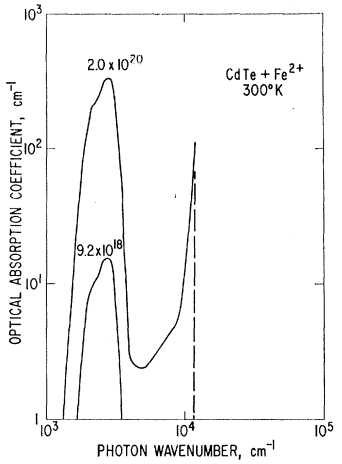

FIG. 7. Optical-absorption coefficient versus photon wave number in the near infrared at 300°K for the two iron-doped CdTe samples studied. The band edge of pure CdTe at $\bar{\nu} \cong 12\,000$ cm^{-1} is shown as the dashed line.

This absorption band at 300°K is shown in Fig. 7 for the two samples studied here. These results are similar to those given previously for different samples, see Fig. 5 of SHC. From the energy level diagrams for a $3d^4$ ion in an octahedral field given by Tanabe and Sugano[22] or McClure,[23] one expects that there will be other optical-absorption bands of Fe^{2+} at photon energies higher than 2400 cm^{-1} wave numbers. The next higher absorption band should occur for $\bar{\nu} \sim 18\,000$ cm^{-1}, where the transition is ^5E to $^3T_1$. We believe we have found

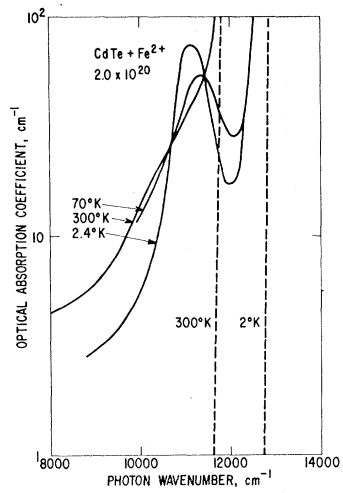

FIG. 8. Optical-absorption coefficient versus photon wave number in the near infrared at several temperatures for CdTe containing 2.0×10^{20} Fe^{2+} ions/cm^3. The nearly vertical dashed line is the band edge of pure CdTe for two different temperatures. The absorption peak at $\bar{\nu} \sim 11\,000$ cm^{-1} is a d-shell transition of the Fe^{2+}.

[22] Y. Tanabe and S. Sugano, J. Phys. Soc. Japan 9, 766 (1954).
[23] D. S. McClure, in *Solid State Physics*, edited by F. Seitz and D. Turnbull (Academic Press Inc., New York, 1959), Vol. 9 p. 399.

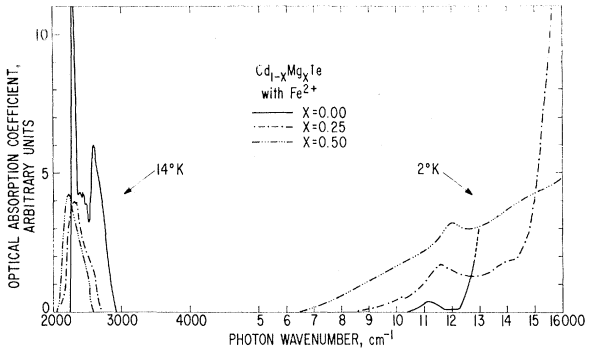

FIG. 9. Optical-absorption coefficient versus photon wave number in the near infrared at low temperatures for iron-doped samples of CdTe-MgTe mixed crystals. The various absorption bands are caused by Fe^{2+}.

this transition at $\bar{\nu} = 11\,200$ cm^{-1}, as shown in Fig. 8. It is very much masked at 300°K by the steeply rising band edge of CdTe. However, at 70 and 2.4°K it is well resolved. In order to demonstrate that this transition is a d-shell transition of the Fe^{2+} and not a d-shell to conduction-band or to valence-band transition, we have studied it in a number of $Cd_{1-x}Mg_xTe$ mixed crystals. In these crystals the band gap increases markedly with the increasing Mg content while the crystal structure stays constant and the lattice parameter changes very little.[24] The rate of change of band gap, E_g, for small x is

$$(1/E_g)(dE_g/dx) = +1.1\,, \qquad (2)$$

based on data of Strauss and Itoh.[24] The rate of change of lattice constant a_0 for small x is

$$(1/a_0)(da_0/dx) = -0.007\,, \qquad (3)$$

based on data of Strauss. Thus the crystal field, which depends on a_0, should stay nearly constant while the band gap E_g changes considerably. The near-infrared optical absorption curves at low temperatures for Fe^{2+} in a series of such mixed crystals is shown in Fig. 9. The samples for $x > 0$ were single crystals grown by Woodbury of this laboratory, and the Fe^{2+} was incorporated by diffusion at 800°C. Since the Fe^{2+} concentration is nonuniform and unknown, the optical absorption coefficient is given arbitrary units. The average Fe^{2+} concentration in these samples is estimated to be 10^{18} to 10^{19} ions of Fe^{2+}/cm^3.

Referring to Tanabe and Sugano[22] and McClure,[23] where their energy level diagrams for d^4 in octahedral symmetry also apply to d^6 in tetrahedral symmetry, we assign the band at $\bar{\nu} \sim 2400$ cm^{-1} to the ^5E to $^5T_2$ transition, and the band at $\bar{\nu} \simeq 11\,500$ cm^{-1} to the ^5E to $^3T_1$ transition. The weak band at $\bar{\nu} \simeq 14\,000$ cm^{-1} may be a ^5E to $^3T_2$ transition, i.e., to a state derived from the ^3P, ^3H free-ion levels. The observed transitions are listed in Table II. The derived energy level scheme for Fe^{2+} in CdTe is shown in Fig. 10. This diagram has been drawn

[24] A. J. Strauss, Bull. Am. Phys. Soc. 13, 453 (1968); K. Itoh, J. Phys. Soc. Japan 22, 1119 (1967).

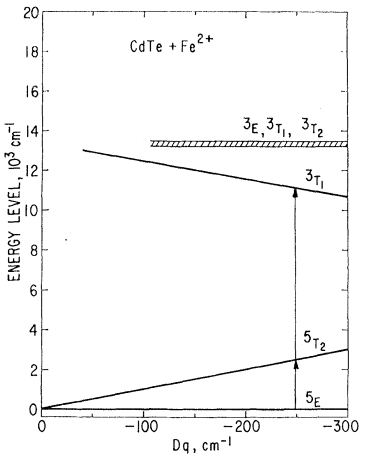

FIG. 10. Various energy levels of Fe^{2+} CdTe as a function of the crystal field parameter Dq. The levels are labeled by their irreducible representations. The two main absorption bands for Fe^{2+} in pure CdTe as shown in Fig. 9 are indicated by the vertical arrows. Pure CdTe has a value of $Dq=-248$ cm^{-1}.

using values for the Racah parameters[22–25] $B=530$ cm^{-1}, $C/B=4.6$. The B values for $x=0.25$ and 0.50 are 2.5% and 5% larger, respectively. These B values are in reasonable agreement with those found[25] for Co^{2+} ions in II–VI compounds. A value of $B=700$ cm^{-1} for Fe^{2+} in ZnS has been found by Marfunin *et al.*,[26] and they have also seen the $^5T_2$, $^3T_1$, $^3T_2$, etc., levels of Fe^{2+}.

In agreement with our prediction of the magnitude of effect of the Mg addition on Dq we find experimentally that

$$(1/Dq)(d(Dq)/dx)=+0.2. \quad (4)$$

Thus Dq changes much less rapidly with x than the band gap [see Eq. (2)].

DISCUSSION OF RESULTS

Phonon Bands in the Far Infrared

The pure, undoped CdTe shows optical-absorption bands in the far-infrared region. These are shown in Figs. 2 and 3 at $\bar{\nu}=71.3$, 92, 104.5, and 114 cm^{-1}. Some plausible assignments of these bands to phonons at critical points in the Brillouin zone can be made; these are shown in Table III. The first three bands listed in Table III are single-phonon bands associated with the X and L critical points.[27] These single-phonon-band absorptions are not allowed in perfect CdTe crystals, but are defect-activated.[28] In zinc blende lattices the defects permit[28] absorption at TA(X), TA(L), and LA(L), but not at LA(X). In Figs. 2 and 3 these three acoustic phonons are seen in the crystals doped with Fe^{2+}. The LA(L) phonon is also seen in pure CdTe, but is much weaker there than in the Fe^{2+}-doped samples. It is believed that the naturally occurring isotopes of both Cd and Te are spread over such a large range of masses and have such large abundances that they serve as defects and permit the LA(L) transition to be seen in the undoped crystal. Somewhat similar allowed bands have been seen in isotopically enriched LiF in the far infrared.[29]

The two-phonon absorption bands are allowed even in pure, isotopically clean CdTe. The selection rules for such bands have been calculated,[30] and, among others, 2TA(L), 2TA(X), LO(X)-TA(X), and LO(L)-TA(L) are allowed in zinc blende structures. The difference band, LO-TA in Table III, is assigned to the absorption of a TA phonon combined with the emission of a second phonon because of the rapid rise of absorption here with increasing temperature. The LO seems the most likely phonon to be involved with the TA because of energy considerations. However, which critical point is involved is unknown. The LO and TO phonons somewhere at the zone boundary have approximate energies[3,19,20,31] of LO$\cong$150 cm^{-1}, TO$\cong$140 cm^{-1}.

TABLE II. Positions of levels $^5T_2$ and $^3T_1$ of Fe^{2+} in $Cd_{1-x}Mg_xTe$ mixed crystals at low temperatures.

Composition x	$^5T_2$ (cm^{-1})	$^3T_1$ (cm^{-1})	$^3T_1$ or $^3T_2$ levels (cm^{-1})
0.0	2480	11 150	?
0.25	2320	11 600	13 900
0.50	2230	12 050	~14 000

TABLE III. Phonon bands in the far-infrared optical absorption of CdTe.

Band wave number (cm^{-1})	Assignment[a]	Crystal
36[b]	TA(L)	Doped with Fe
46[b]	TA(X)	Doped with Fe
104.5	LA(L)	Pure[c]
71.3	2TA(L)	Pure and doped
92	2TA(X)	Pure
114	LO-TA[d]	Pure

[a] TA = transverse acoustic, LA = longitudinal acoustic, LO = longitudinal optic, and X, L = critical points in the Brillouin zone.
[b] The presence of these two bands is less certain than the others because of their small optical-absorption coefficient (maximum $\alpha<1$ cm^{-1}).
[c] Very strong absorption for this band in the Fe-doped crystal.
[d] Critical point uncertain.

[25] J. M. Baranowski, J. W. Allen, and G. L. Pearson, Phys. Rev. **160**, 627 (1967).
[26] A. S. Marfunin, A. N. Platonov, and V. E. Fedorov, Fiz. Tverd. Tela **9**, 3616 (1967) [English translation: Soviet Phys.—Solid State **9**, 2847 (1968)].
[27] R. H. Parmenter, Phys. Rev. **100**, 573 (1955).
[28] R. Loudon, Proc. Phys. Soc. (London) **84**, 379 (1964).
[29] M. V. Klein and H. F. MacDonald, Phys. Rev. Letters **20**, 1031 (1968).
[30] J. L. Birman, Phys. Rev. **131**, 1489 (1963).
[31] A. Mooradian and G. B. Wright, Bull. Am. Phys. Soc. **13**, 480 (1968). The phonon energies given in the abstract were corrected verbally to give TA=35 cm^{-1}, LA=97 cm^{-1}, TO=139 cm^{-1}, LO=150 cm^{-1}. See also *Proceedings of the Ninth International Conference on the Physics of Semiconductors, Moscow, July, 1968* (Publishing House Nauka, Leningrad, 1968), p. 1020, where they give TA=35 cm^{-1}, LA=97 cm^{-1}, TO=151 cm^{-1}, and LO=118 cm^{-1}. Apparently some difficulty exists in the assignment of phonon energies.

With the assignment of phonon energies as given in Table III we are in only fair agreement with previous assignments[19,20,31] for the TA and LA phonon energies at the zone boundary. The previous assignment of SHC for TA=65 cm^{-1} is now seen to be incorrect. The major difference between the present assignment and previous ones is the realization that more than one TA or LA phonon energy may exist. Indeed there are three critical points[30] at X, L, and W, each of which may be important. The present assignment may also be compared to results for critical point phonon energies in InSb, which has the same structure and atoms of nearly the same mass as CdTe. Stierwalt[32] finds TA(L)=34 cm^{-1}, TA(X)=41.5 cm^{-1}, LA(L)=102 cm^{-1}, for InSb, in quite good agreement with Table III for CdTe.

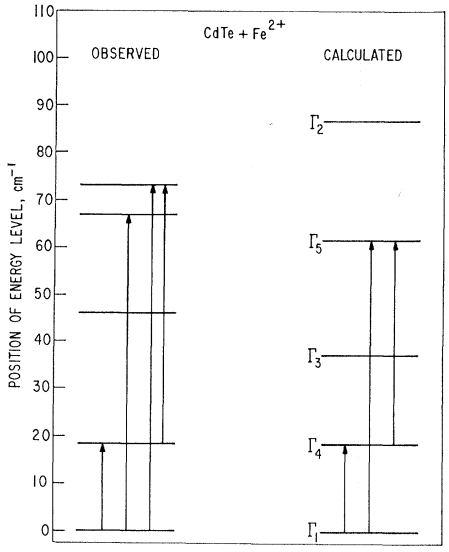

FIG. 11. Observed and calculated energy levels of the ^5E state of Fe^{2+} in CdTe in the far-infrared region in zero magnetic field. The observed optical transitions are shown by the vertical arrows on the left-hand side; the theoretically allowed transitions are shown on the right-hand side.

Fe^{2+} Bands in the Far Infrared

In Figs. 2 and 3 the optical-absorption peaks at $\bar{\nu}$=18.6, 54.8, 66.7, and 73.2 cm^{-1} are believed to be associated with electronic transitions of the Fe^{2+} impurities in tetrahedral lattice sites. The assignments are listed in Table IV. The purely electronic transitions at $\bar{\nu}$=18.6, 54.8, 66.7, and 73.2 cm^{-1} are very similar to those seen for Fe^{2+} in cubic ZnS by SRH. In SRH the energy level spectrum and the allowed optical transitions for the ^5E state of tetrahedral Fe^{2+}, $3d^6$ were given. The results for ZnS in SRH were not complicated by the presence of nearby phonon absorption bands, because the phonon energies in ZnS are much larger.[3] Thus the analysis was much easier. The CdTe+Fe^{2+} spectrum is much more complex for $0<\bar{\nu}<120$ cm^{-1} than that of ZnS+Fe^{2+}. In particular the transition at $\bar{\nu}$=73.2 cm^{-1} is nearly masked by the $2TA(L)$ band at $\bar{\nu}$=71.3 cm^{-1} at low Fe^{2+} concentrations (see Fig. 2). At high Fe^{2+} concentrations, as in Fig. 3, it becomes comparable in intensity to the $2TA(L)$ at 4.2°K.

[32] D. L. Stierwalt, J. Phys. Soc. Japan Suppl. **21**, 58 (1966).

TABLE IV. Fe^{2+} bands in the far-infrared optical absorption of doped CdTe.

Band wave number (cm^{-1})	Transition assignment	Oscillator strength measured
18.6	($\Gamma_1-\Gamma_4$)	1.5×10^{-8}
54.8	(Γ_4 to 73.2 cm^{-1})	
66.7		3×10^{-8}
73.2	($\Gamma_1-\Gamma_5$)?	3×10^{-8}

The two assignments in Table IV can be justified on the bases of the energies for the particular transitions, their selection rules, the temperature dependence of the bands, their oscillator strengths, and finally their splitting in a magnetic field. The experimental values for the energies of five different levels of Fe^{2+} in CdTe are shown in Fig. 11. The positions of all of the levels except the one at 46 cm^{-1} are from the present far-infrared data. The position of level Γ_3 is difficult to determine from the far-infrared absorption since $\Gamma_1-\Gamma_3$ transitions are forbidden (see SRH). The position of the level at 46 cm^{-1} has been measured from near-infrared studies of hot electron effects[33] on the optical absorption. This level, which we believe is the Γ_3 level, occurs at 46 ± 2 cm^{-1} above level Γ_1. These energies are compared in Fig. 11 with the theoretical predictions given in the Appendix. The simplest theory predicts that the levels should be equally spaced by an amount, K, where

$$K=6\lambda^2/\Delta. \tag{5}$$

Here λ=spin-orbit coupling parameter, and $\Delta=|10\,Dq|$=energy separation between the ^5E and $^5T_2$ states. Using $\lambda=-100$ cm^{-1} for Fe^{2+} and $\Delta=+2480$ cm^{-1} (see SHC) we obtain K=24.19 cm^{-1}. The calculations in the Appendix for the energy levels of the ^5E state are summarized in Table V. These show that the

TABLE V. The computed energy levels of the ^5E state of Fe^{2+} in CdTe using $\lambda=-100$ cm^{-1}, $Dq=-248$ cm^{-1}. The lowest level, Γ_1, is taken as the zero reference. Here $K=6\lambda^2/\Delta=24.19$ cm^{-1}, $\sigma=|\lambda|/\Delta=+0.04032$, and $\Delta=|10\,Dq|$.

Level Irr. rep.	Energy of the level Perturbation theory	Exact
Γ_1	$0=0.00$	0.00
Γ_4	$K(1-5\sigma)=19.32$	18.57
Γ_3	$2K(1-5\sigma)=38.64$	37.35
Γ_5	$3K(1-3\sigma)=63.81$	61.55
Γ_2	$4K(1-2\sigma)=88.97$	86.74

[33] G. E. Fenner, G. A. Slack, and J. T. Vallin, in *Proceedings of the Ninth International Conference on the Physics of Semiconductors, Moscow, July, 1968* (Publishing House Nauka, Leningrad, 1968), p. 1180.

five levels are equally spaced by multiples of K only when $\sigma \ll 1$, where $\sigma = |\lambda|/\Delta$. The present value of $\sigma = +0.0403$ is not sufficiently small for this to be the case (see Table V). The exact calculation of the level positions, as described in the Appendix, gives the values in the last column of Table V. These values are plotted in Fig. 11 together with the experimental ones. Note that the calculated position of the Γ_4 level (18.57 cm^{-1}) is in good agreement with the observed value (18.62 cm^{-1}). The agreement for the Γ_3 level is not as good, while experimentally the Γ_5 level appears actually to be a doublet centered about $\bar{\nu} = 70$ cm^{-1} instead of a single line at 61.55 cm^{-1}. The reason for this discrepancy is uncertain, but it may be connected with possible interactions of the electronic Γ_5 level with the low-energy TA phonons at 36 and 46 cm^{-1}, i.e., vibronic or dynamic Jahn-Teller effects.

Fe^{2+} Bands in Near Infrared

The present values for the phonon energies in CdTe are in disagreement with earlier ones on Fe^{2+} in CdTe by SHC. Furthermore in SHC the value of K was given as 10 ± 2 cm^{-1}. This incorrect value was based on a misidentification of the lines at $\bar{\nu} = 2273$, 2274, and 2250 cm^{-1}. The new assignments are given in Table VI where the derived energies for levels No. 1, 2, 3, 6, 7, and 8 are at 0, 19, 44, 2282, 2294, and 2309 cm^{-1}, respectively. These results agree with Baranowski *et al.*[25] who find levels No. 1, 2, and 6 at 0, 17, and 2282 cm^{-1}. The demarcation between zero-phonon lines and phonon-assisted transitions now occurs at $\bar{\nu} = 2314$ cm^{-1}, not at 2340 cm^{-1} as in SHC. This new analysis yields only three levels, i.e., Nos. 6, 7, and 8 in the $^5T_2$ state for which zero-phonon optical transitions from the Γ_1 ground level of the ^5E state are seen. The former levels labeled Nos. 9 and 10 are now seen to be associated with phonon-assisted transitions.

TABLE VI. Assignments of optical-absorption bands and energy levels of Fe^{2+}-doped CdTe in the near infrared.

Band wave number (cm^{-1})	Old assignment SHC-Ref. 3	Present assignment (a)
2250	(4–6)	(3–7)
2264	(3–6)	(2–6)
2273	(2–6)	(2–7)
2282	(1–6)	(1–6)
2294	(1–7)	(1–7)
2309	(1–8)	(1–8)
2318	(1–9)	(1–6)+TA(L)
2334	(1–10)	(1–7)+TA(L)
2346	(1–6)+TA	(1–8)+TA(L)
2355	(1–7)+TA	(1–6)+2TA(L)
2371	(1–8)+TA	(1–7)+2TA(L)
2388	(1–6)+LA	(1–6)+LA(L)
2397	(1–7)+LA	(1–7)+LA(L)

[a] Levels 1–3 are the Γ_1, Γ_4, and Γ_3 levels, respectively, of the ^5E state. Levels 6, 7, and 8 belong to the $^5T_2$ state, but their irreducible representations are uncertain.

Fe^{2+} Line at $\bar{\nu} = 18.6$ cm^{-1}

The $\Gamma_1 - \Gamma_4$ transition at $\bar{\nu} = 18.6$ cm^{-1} is sufficiently far removed from the phonon-absorption peaks so that some unambiguous measurements can be made. The integrated absorption values, A [see Eq. (1)], at 4.2°K from Figs. 2 and 3 are 0.68 cm^{-2} and 10.5 cm^{-2}, respectively. The values can be converted to a normalized intensity, I [see Eq. (3) of SRH], where N = the measured concentration of Fe^{2+} ions per unit volume. For this conversion we need the far-infrared refractive index, n. The literature value[34,35] at 4°K is $n^2 = 9.7$. Further unpublished interference-fringe measurements[36] on a pure CdTe single crystal at 9°K in the far-infrared region $10 < \bar{\nu} < 60$ cm^{-1} gave $n^2 = 9.65$. Using $n^2 = 9.7$ the values of I, which is a dimensionless quantity, are 1.7×10^{-8} for Fig. 2 and 1.3×10^{-8} for Fig. 3 at 4.2°K. From Eq. (21) of SRH these results give nearly the same numerical values for the experimental oscillator strength of the $\bar{\nu} = 18.6$ cm^{-1} transition, or an average of

$$f(\Gamma_1,\Gamma_4) = (1.5 \pm 0.2) \times 10^{-8} \quad (6)$$

(see Table IV). The theoretical value for this magnetic dipole transition can be calculated from Eqs. (16) and (17) of SRH. This gives

$$f_m(\Gamma_1,\Gamma_4) = 1.2 \times 10^{-8}, \quad (7)$$

in very good agreement with the experimental value. In a similar fashion the oscillator strengths for the transitions at $\bar{\nu} = 66.7$ and 73.2 cm^{-1} can be estimated from Fig. 3. The experimental values for the two transitions are nearly the same, and are

$$f(66.7\ cm^{-1}) \cong f(73.2\ cm^{-1}) = (3 \pm 1) \times 10^{-8}. \quad (8)$$

A theoretical estimate of these oscillator strengths is not possible now because we do not know the nature of the optical transitions. However, these values are comparable to $f = 4 \times 10^{-8}$ found for the $(\Gamma_1 - \Gamma_5)$ transition of Fe^{2+} in ZnS, see Table IV of SRH.

The Γ_4 level is triply degenerate in zero magnetic field while the Γ_1 level is a singlet. The Γ_4 level will split into three component levels in an applied magnetic field. The splitting as a function of magnetic induction has been calculated exactly in the Appendix. The results are shown in Fig. 12 for a field along a $\langle 100 \rangle$ axis. For a longitudinal applied field as in Fig. 4(a), theory predicts that optical transitions are allowed from Γ_1 to the upper and lower components (i.e., levels Nos. 8 and 14 of Fig. 12) of Γ_4, but not to the middle one (No. 3). The results in Fig. 5(a) agree with this prediction. For a transverse field as in Fig. 4(b), optical transitions are allowed to all three components, in agreement with

[34] D. Berlincourt, H. Jaffe, and L. R. Shiozawa, Phys. Rev. **129**, 1009 (1963).
[35] B. Segall, M. R. Lorenz, and R. E. Halsted, Phys. Rev. **129**, 2471 (1963).
[36] S. Roberts and D. T. Marple, in *Physics and Chemistry of II-VI Compounds*, edited by M. Aven and J. S. Prener (North-Holland Publishing Co., Amsterdam, 1967), p. 335.

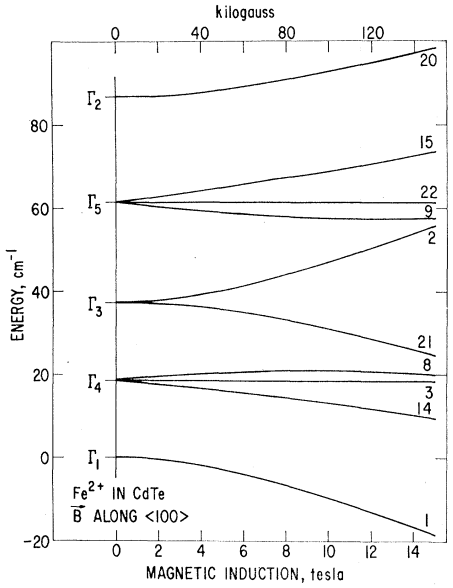

FIG. 12. Splitting of the five levels of the ^5E state of Fe^{2+} in CdTe in a ⟨100⟩ applied magnetic field. The ordinate is the energy in wave numbers and the abcissa the magnetic induction, B, in T (kG). For this plot the energies have been calculated exactly from Eqs. (A12) and Table XI. The mixing of the wave functions from the $^5T_2$ state has therefore been included. The numbers on the right-hand side indicate the i in $\tilde{\Psi}_i$ for the level.

Fig. 5(b). The experimental positions of the various absorption peaks as a function of the magnetic induction are given in Table I. In Fig. 12 all of the levels except Nos. 3 and 22 shift with B, and this shift can be written as a power series in the magnetic induction, B, as

$$\Delta E = a_1 B + a_2 B^2 + a_3 B^3 .$$

Only levels Nos. 8, 9, 14, and 15 have a nonzero a_1 coefficient. Also for the pair (Nos. 8 and 14) the a_2 coefficients are nearly identical. Thus, if we designate their respective energies by E_8 and E_{14}, the difference $E_8 - E_{14}$ is linear in B to $\pm 1\%$ up to about 3 T. We define

$$g(\Gamma_4) = \lim_{B\to 0}[E_8 - E_{14}]/2\beta B , \qquad (9)$$

where β = the Bohr magneton $= 0.92732\times 10^{-23}$ J/T, B = magnetic induction in T, 1 T $= 10^4$ G, $g(\Gamma_4)$ = the effective gyromagnetic ratio of the Γ_4 level. Equation (9) was derived for B along any ⟨100⟩ axis. However, $g(\Gamma_4)$ is isotropic, and hence Eq. (9) applies to our unoriented oligocrystalline sample. The experimental value of $g(\Gamma_4)$ from Fig. 6 is

$$g(\Gamma_4) = 1.02 \pm 0.04 , \qquad (10)$$

where the uncertainty in both $\bar{\nu}_h - \bar{\nu}_l$ and B has been taken into account. The theoretical value of $g(\Gamma_4)$ from the exact calculation in the Appendix is

$$g(\Gamma_4) = 0.940 . \qquad (11)$$

The difference between Eqs. (10) and (11) is just outside the experimental uncertainty, but is not considered to be particularly significant.

The theoretical value of $g(\Gamma_5)$ from the Appendix is

$$g(\Gamma_5) = 1.305 , \qquad (12)$$

significantly larger than $g(\Gamma_4)$. Unfortunately, the lines at $\bar{\nu} = 66.7$ and 73.2 cm^{-1} are rather broad and partially masked by lattice bands, so no experimental determination of $g(\Gamma_5)$ was made.

Another noticeable feature of the $\bar{\nu} = 18.6$ cm^{-1} line in Figs. 5(a) and 5(b) and in Table I is the shift of both $\bar{\nu}_c$ and $\frac{1}{2}(\bar{\nu}_h + \bar{\nu}_l)$ to higher wave numbers with increasing magnetic field. This is explained by the rapid decrease of the Γ_1 level in Fig. 12 with increasing field. For small values of B (i.e., $B < 3$ T) this decrease is independent of crystallographic orientation and has a theoretical value (see Appendix) of

$$E_1 = -0.122 B^2 \text{ cm}^{-1} , \qquad (13)$$

where B is in T. At $B = 2.4$ T, Eq. (13) gives $E_1 = -0.70$ cm^{-1}, which is comparable to the observed value of -0.49 cm^{-1} at 2.4 T from Table I for the shift of $\bar{\nu}_c$.

Magnetic Susceptibility

The magnetic susceptibility χ of an unoriented, polycrystalline sample of iron-doped CdTe was measured[37] from 4 to 150°K for values of magnetic induction B up to 2 T. The χ was independent of B up to 2 T. The CdTe sample contained 9.2×10^{18} Fe^{2+}/cm^3. In order to determine the paramagnetic χ of only the Fe^{2+}, the diamagnetic susceptibility of pure, undoped CdTe was also determined and the necessary subtraction was made. From 4 to 150°K the χ_M per mole of CdTe (not Fe) for undoped CdTe was nearly independent of temperature and its value was

$$\chi_M = -9.8\times 10^{-10} \text{ (m}^3\text{/mole)},$$
$$\text{or } -7.8\times 10^{-5} \text{ (emu/mole)}.$$

The χ versus T curve for Fe^{2+} is shown in Fig. 13. The experimental curve is somewhat uncertain below 8°K, and is shown as a dashed line. Once the energy levels as a function of B are known (see Fig. 12), then the χ can be calculated exactly. This was done using Eq. (A17) and the exact values of the constants in Table VII (see Appendix). These results are also shown in Fig. 13. There are no adjustable parameters in this theoretical curve. In the limit as $T \to 0$°K the theory gives

$$\chi_{MO} = +3.679\times 10^{-6} \text{ (m}^3\text{/mole)} \qquad (14)$$

from Eqs. (A20) and (A21). With the measured Fe^{2+} concentration of 15.2 mole/m^3 this converts, see Eq. (A17), to

$$\chi_{VO} = +5.60\times 10^{-5} , \qquad (15)$$

[37] We are indebted to I. S. Jacobs, J. B. Comly, and J. Kenyon of this laboratory for these measurements.

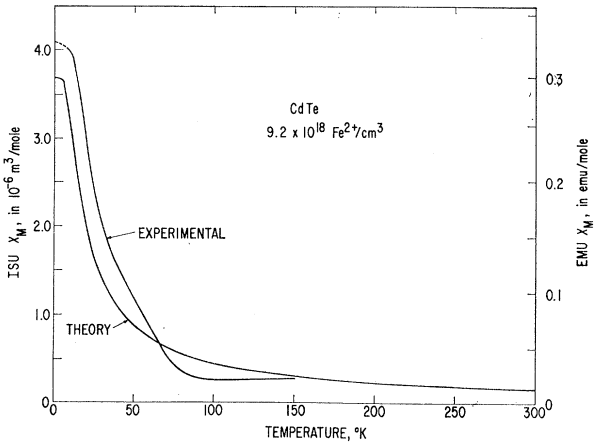

FIG. 13. Magnetic susceptibility of Fe^{2+} in CdTe versus temperature, both experimental and theoretical curves are given. The left-hand ordinate gives the susceptibility per mole of Fe^{2+} ions in the International System of Units. The right-hand ordinate gives the same quantity in electromagnetic units. These are related by a factor of $(10^6/4\pi)$.

which is expressed in the SI and is dimensionless. The experimental value of $\chi_{MO}(0°K)$ is only 11% larger than the theoretical. This agreement at 0°K depends only on the properties of the Γ_1 state, and shows that its predicted behavior of energy versus magnetic induction is well obeyed. As can be seen from Fig. 13 the agreement between theory and experiment is quite good. The differences are quite acceptable in view of some uncertainty about the Fe^{2+} concentration, and in view of the fact that at such a low Fe concentration we were at about the limit of the sensitivity of the magnetometer.

The temperature dependence of χ in Fig. 13 can be broken up into several regions. For $T<5°K$ χ is dominated by the Γ_1 level, and χ_{MO} is determined solely by this Γ_1 level. For $5°K<T<40°K$ the χ versus T curve is dominated by the Γ_1 and Γ_4 levels, and the good agreement is indicative of proper theoretical values for these levels. For $T>40°K$ the computed χ versus T behavior is sensitive to the presence of the Γ_3, Γ_5, and Γ_2 levels. The match between theory and experiment is not as good for $T>40°K$ as at lower temperatures. However, it is clear from the experimental χ versus T curve that there are some levels above the Γ_4, and that the theory is about right for their energies versus magnetic field.

TABLE VII. Numerical constants in Eq. (A17) for the magnetic susceptibility of Fe^{2+} in CdTe.

Quantity	Irr. rep. of level	Value of quantity Approximate	Exact
e_1	Γ_1	0	0
e_4	Γ_4	1	+1.0000
e_3	Γ_3	2	+2.0112
e_5	Γ_5	$3(1+2\sigma)$	+3.3143
e_2	Γ_2	$4(1+3\sigma)$	+4.6711
n_1	Γ_1	1	+1
n_4	Γ_4	$\frac{1}{8}[(x+3)-3\sigma(4x+7)]$	$+0.2792+0.0848x$
n_3	Γ_3	-14σ	−0.4205
n_5	Γ_5	$\frac{1}{8}[(x-3)+\sigma(4x+21)]$	$-0.2792+0.1633x$
n_2	Γ_2	$-1+14\sigma$	−0.5544
p_1	Γ_1	1	1
p_4	Γ_4	3	3
p_3	Γ_3	2	2
p_5	Γ_5	3	3
p_2	Γ_2	1	1

A χ which is independent of magnetic field corresponds to an induced dipole moment proportional to field. In the limit as $T\rightarrow 0°K$ the theoretical value of this induced moment from Eqs. (A20) and (A21) is 0.5241 Bohr magnetons for one Fe^{2+} ion at a magnetic induction of $B=1$ T.

In order to relate to the more commonly used electromagnetic units (emu)[38] we note that 1 T = 10 kG, and that

$$\chi_V(\mathrm{SI})=4\pi\chi_V(\mathrm{emu}). \tag{16}$$

This latter relation exists because in the SI

$$\mathbf{B}=\mu_0(\mathbf{H}+\mathbf{M}), \tag{17}$$

whereas in emu

$$\mathbf{B}=\mathbf{H}+4\pi\mathbf{M}. \tag{18}$$

CONCLUSIONS

The optical-absorption and magnetic susceptibility studies of Fe^{2+} in CdTe agree with a model in which the Fe^{2+} ion enters substitutionally for a Cd ion. The energy levels of the Fe^{2+} in this environment are then determined by the electrostatic crystal field of the four surrounding Te ions. The lowest level of the ^5E state is a Γ_1 singlet, and the next higher level is a Γ_4 triplet. The theoretical calculations of the energy separation, 18.57 cm^{-1}, of the gyromagnetic ratio, $g(\Gamma_4)=0.940$, of the low-temperature susceptibility, $\chi_{MO}=+3.68\times10^{-6}$ (m^3/mole), and of the oscillator strength $f(\Gamma_1,\Gamma_4)=1.16\times10^{-8}$, show good agreement with experimental values.

The experimental confirmation of the energies and magnetic field properties of the higher levels, i.e., Γ_3, Γ_5, and Γ_2, is considerably poorer. However, both the optical-absorption coefficient and magnetic susceptibility measurements show that these levels do exist, but their energies and degeneracies are somewhat uncertain. For example, the presence of two levels at 66.7 and 73.2 cm^{-1}, found optically, does not agree well with the theoretical prediction of one level at 61.55 cm^{-1}. The correct explanation of this difference may involve vibronic effects with some of the low-energy TA phonon modes of CdTe.

Optical studies in the near infrared indicate a $^5T_2$ band of Fe^{2+} centered at $\bar{\nu}=2480$ cm^{-1} (see SHC) with three levels at 2282, 2294, and 2309 cm^{-1} to which zero-phonon transitions from the Γ_1 ground state are allowed. There is also an additional $^3T_1$ band centered at 11 150 cm^{-1}.

The far-infrared studies also give energies for some of the phonons at critical points in the Brillouin zone.

[38] J. H. Van Vleck, *The Theory of Electric and Magnetic Susceptibilities* (Clarendon Press, Oxford, England, 1932).

These are TA(L)=36 cm^{-1}, TA(X)=46 cm^{-1}, LA(L) =104.5 cm^{-1}.

Note added in proof. Recent work of C. T. Sennett, D. R. Bosomworth, W. Hayes, and A. R. L. Spray in J. Phys. C **2**, 1137 (1969) are in good agreement with the results in Fig. 2 and Table III.

ACKNOWLEDGMENTS

The authors would like to thank F. S. Ham for his help with the theoretical calculations; I. S. Jacobs, J. B. Comly, and Jean W. Kenyon for their magnetic susceptibility measurements; S. V. Galginaitis and H. H. Woodbury for growing the crystals; D. T. F. Marple for the loan of an optical cryostat; and J. H. McTaggart for his aid in many phases of the work.

APPENDIX

Experiments have shown that the crystal field splitting for Fe^{2+} ($3d^6$) in II–VI compounds is considerably smaller than the separation of the LS terms for the free ion. Therefore, one can expect that the lowest levels for the Fe^{2+} ion in a crystal will originate from the free ion ^5D ground state.[39] Our Hamiltonian can be written as[40]

$$\mathcal{H}=\mathcal{H}_F+\lambda\mathbf{L}\cdot\mathbf{S}+\mathcal{H}_{CF}, \tag{A1}$$

where $\mathcal{H}_F$ is the free-ion Hamiltonian exclusive of spin-orbit interactions, $\lambda\mathbf{L}\cdot\mathbf{S}$ is the spin-orbit interaction, and $\mathcal{H}_{CF}$ is the perturbation due to the crystal field. Since the cubic crystal field splitting is larger than the spin-orbit interaction in iron, we will introduce $\mathcal{H}_{CF}$ due to the crystal field before we consider the spin-orbit interaction.

Crystal Field

In tetrahedral symmetry the free-ion orbital D state, which is five-fold degenerate, will, according to group theory, split into an orbital doublet E and an orbital triplet T_2. The crystal field potential as given by Griffiths[40] and Hutchings[41] for a T_d crystal, see Fig. 14, is

$$V_{\text{crystal}}=F(r)[Y_4^0+(5/14)^{1/2}(Y_4^4+Y_4^{-4})], \tag{A2}$$

where the Y_L^M are spherical harmonics.[40,41] Low and Weger[1] have given the Y_4^4 coefficient as $-(5/14)^{1/2}$ instead of $+(5/14)^{1/2}$. This mistake makes many of their results incorrect. This mistake can be superficially corrected by relating their results to a coordinate system in which the $\Phi=0$ line is a [110] axis instead of a [100] (see Fig. 14).

Now we assume that the wave function of the orbital E and orbital T_2 states of the Fe^{2+}, $3d^6$ ion in T_d symmetry originate from the lowest free-ion ^5D level. No intermixing of d^5p and d^5f configurations is considered, as suggested and then rejected by Low and Weger.[1] This means the wave functions are, except for a radial part, linear combinations of the spherical harmonics Y_2^M, where ($M=M_L=0, \pm1, \pm2$). The coordinate system used is shown in Fig. 14. From the Hamiltonian, Eq. (A1), with $\lambda=0$ we get a 5×5 matrix. Its solution is an orbital doublet E-state at energy $\langle E|\mathcal{H}_{CF}|E\rangle=6\,Dq$ and an orbital triplet T_2 state at energy $\langle T_2|\mathcal{H}_{CF}|T_2\rangle=-4\,Dq$. Where the energy difference is, by definition, $|10\,Dq|$. In T_d symmetry the E state of Fe^{2+} is lower in energy so $Dq<0$.

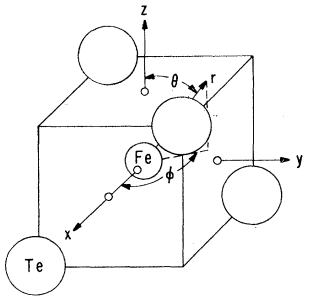

FIG. 14. Geometrical configuration of an Fe atom surrounded tetrahedrally by 4 Te atoms. The rectangular and polar coordinate systems are shown.

The basis functions for the orbital E state are

$$\begin{aligned} Y_2^0&=a(3z^2-r^2)/\sqrt{6}\,,\\ (1/\sqrt{2})(Y_2^2+Y_2^{-2})&=a[\sqrt{3}\,(x^2-y^2)]/\sqrt{6}\,, \end{aligned} \tag{A3}$$

while the basis functions for the orbital T_2 state are the triplet

$$\begin{aligned} Y_2^1&=a(-xz-iyz)\,,\\ Y_2^{-1}&=a(xz-iyz)\,,\\ (1/\sqrt{2})(Y_2^2-Y_2^{-2})&=a(i\sqrt{2}xy)\,, \end{aligned} \tag{A4}$$

where the constant $a=[\sqrt{30\pi}]/4\pi r^2$. We have expressed the spherical harmonics in terms of x, y, and z in order to make use of the tables of Koster *et al.*[42]

Spin-Orbit Coupling

As long as spin-dependent terms are not included in the Hamiltonian each orbital wave function will be five-fold degenerate due to the spin $S=2$ of the $3d^6$ system. In T_d symmetry the spin functions S_2^M ($M=M_s=0, \pm1, \pm2$) may be grouped into E and T_2 functions in a way similar to the orbital functions. The combined spin-orbit wave functions of the ^5D free-ion state are twenty-five-fold degenerate. From the T_d group multiplication table[42] one obtains for

$$^5E\text{:}\quad E\times(E+T_2)=\Gamma_1+\Gamma_2+\Gamma_3+\Gamma_4+\Gamma_5$$

and for $^5T_2$: (A5)

$$T_2\times(E+T_2)=\Gamma_1+\Gamma_3+2\Gamma_4+2\Gamma_5\,.$$

[39] C. E. Moore, *Atomic Energy Levels* (U. S. Government Printing Office, Washington, D. C., 1952), Vol. 2, p. 60.

[40] J. S. Griffith, *The Theory of Transition-Metal Ions* (Cambridge University Press, Cambridge, England, 1961), Chap. 8.

[41] M. T. Hutchings, in *Solid State Physics*, edited by F. Seitz and D. Turnbull (Academic Press Inc., New York, 1964), Vol. 16, p. 227.

[42] G. F. Koster, J. O. Dimmock, R. G. Wheeler, and H. Statz, *Properties of the Thirty-Two Point Groups* (MIT Press, Cambridge, Mass., 1963).

Thus the orbital ^5E state yields five irreducible representations while the $^5T_2$ yields six. We have used Mulliken's notation for the irreducible representations (E,T_2) for the separate orbital and spin functions while for the combined spin-orbit wave functions we use Bethe's notations (Γ_1, Γ_2 etc.; see SHC). By use of the tables of coupling coefficients given by Koster *et al.*[42] we can write down the spin-orbit product wave functions for the 25 individual levels explicitly and can find the irreducible representations to which they belong. For example the singlet Γ_2 wave function for the orbital ^5E state is given by

$$\Psi_{20}=\tfrac{1}{2}[(Y_2^2+Y_2^{-2})S_2^0-Y_2^0(S_2^2+S_2^{-2})], \quad \text{(A6)}$$

where the Y terms are the orbital spherical harmonics and the S terms are the spin spherical harmonics. This is abbreviated by using the kets $|M_LM_S\rangle$ as

$$\Psi_{20}=\tfrac{1}{2}[+|20\rangle-|02\rangle-|0\bar{2}\rangle+|\bar{2}0\rangle], \quad \text{(A7)}$$

where the $|0\bar{2}\rangle$ means $M_L=0$, $M_S=-2$. The 25 wave functions so obtained are given in Tables VIII and IX.

The inclusion of the spin-orbit coupling term $\lambda\mathbf{L}\cdot\mathbf{S}$ in Eq. (A1) now makes the matrix $\langle\Psi_i|\mathcal{H}|\Psi_i\rangle$ a 25×25 matrix ($1\leq i\leq25$). Low and Weger[1] show that this matrix breaks up into one 7×7 and three 6×6 matrices. Because the Hamiltonian Eq. (A1) does not give any coupling between wave functions belonging to different irreducible representations, we can see from Eq. (A5) that the 25×25 matrix can be reduced to one 1×1, two 2×2, and six 3×3 matrices. The 1×1 matrix is the Γ_2 for Ψ_{20} at an energy of 6 Dq. The others are

$$\Gamma_1:\quad \begin{array}{c|cc} i\backslash j & 1 & 7 \\ 1 & 6\,\mathrm{Dq} & -2w\lambda \\ 7 & -2w\lambda & -4\,\mathrm{Dq}-2\lambda \end{array}$$

$$\Gamma_3:\quad \begin{array}{c|cc} i\backslash j & 2 & 5 \\ 2 & 6\,\mathrm{Dq} & 2v\lambda \\ 5 & 2v\lambda & -4\,\mathrm{Dq}+\lambda \end{array}$$

for (2,5) or (21,24),

$$\Gamma_4:\quad \begin{array}{c|ccc} i\backslash j & 3 & 4 & 6 \\ 3 & 6\,\mathrm{Dq} & w\lambda & -2v\lambda \\ 4 & w\lambda & -4\,\mathrm{Dq}+\lambda & 0 \\ 6 & -2v\lambda & 0 & -4\,\mathrm{Dq}-2\lambda \end{array} \quad \text{(A8)}$$

for (3,4,6) or (8,11,13) or (14,17,19),

$$\Gamma_5:\quad \begin{array}{c|ccc} i\backslash j & 9 & 10 & 12 \\ 9 & 6\,\mathrm{Dq} & s\lambda & -t\lambda \\ 10 & s\lambda & -4\,\mathrm{Dq}+3\lambda & 0 \\ 12 & -t\lambda & 0 & -4\,\mathrm{Dq}-2\lambda \end{array}$$

for (9,10,12) or (15,16,18) or (22,23,25),

where $s=(18/5)^{1/2}$, $t=(12/5)^{1/2}$, $u=\sqrt{2}$, $v=\sqrt{3}$, and $w=\sqrt{6}$. The entries in the matrices are just $\langle\Psi_i|\mathcal{H}|\Psi_j\rangle$ for various i and j where $1\leq i,\ j\leq25$. The Γ_3 matrix in Eq. (A8) shows the interaction between Ψ_2 and Ψ_5 (as given in Tables VIII and IX). It also holds when both $i=2$ is replaced by $i=21$ and 5 is replaced by 24. Similar replacements are shown in Eq. (A8) for the Γ_4 and Γ_5 matrices. The matrices in Eq. (A8) only couple those wave functions that have the same transformation basis functions. Thus Ψ_2 and Ψ_5 in the Γ_3 matrix transform as $(3z^2-r^2)$, as indicated in Tables VIII and IX. The basis functions are taken from Koster *et al.*[42]

These 2×2 and 3×3 matrices can be solved exactly for the eigenenergies and eigenfunctions. Approximate values can also be obtained by perturbation theory. The perturbation theory calculation gives the lowest energy level as the Γ_1 of the ^5E state at

$$E^0(\Gamma_1)=-6|\mathrm{Dq}|\,(1+40\sigma^2-80\sigma^3), \quad \text{(A9)}$$

where $\sigma=|\lambda/10\,\mathrm{Dq}|$, referred to the ^5D free-ion state as zero. If the zero is readjusted to make $E_1=0$, then the other levels lie at the energies given in Table V. The exact calculation gives $E^0(\Gamma_1)=-1575$ cm^{-1} below the free-ion level.

Note that the levels of Table V are all spaced approximately 20 cm^{-1} apart. This spacing of about $K=6\lambda^2/\Delta$, although a second-order effect in λ, is relatively large and is made so by the relatively small value of Δ for CdTe.

The eigenfunctions corresponding to the eigenenergies are not simply the Ψ_i given in Tables VIII and IX, but are linear combinations of these Ψ_i. Let us denote these eigenfunctions by $\tilde{\Psi}_i$, where we have for the ^5E state

$$\begin{aligned} &\Gamma_1:\quad \tilde{\Psi}_1=c_1\Psi_1+c_7\Psi_7, \\ &\Gamma_4:\quad \tilde{\Psi}_3=c_3\Psi_3+c_4\Psi_4+c_6\Psi_6, \\ &\Gamma_3:\quad \tilde{\Psi}_2=c_2\Psi_2+c_5\Psi_5, \\ &\Gamma_5:\quad \tilde{\Psi}_9=c_9\Psi_9+c_{10}\Psi_{10}+c_{12}\Psi_{12}, \\ &\Gamma_2:\quad \tilde{\Psi}_{20}=c_{20}\Psi_{20}. \end{aligned} \quad \text{(A10)}$$

In Eq. (A10) we have the same replacement possibilities on the index i as in Eq. (A8). Thus, for example,

$$\tilde{\Psi}_8=c_3\Psi_8+c_4\Psi_{11}+c_6\Psi_{13}$$

and so forth. An exact calculation gives the values of c_i shown in Table X. Note that the values in the third column of Table X are all close to unity, which means that $\tilde{\Psi}_i$ is a moderately close approximation to Ψ_i. The fifth and seventh columns of Table X show that the amount of mixing of $^5T_2$ wave functions into the $\tilde{\Psi}_1$, $\tilde{\Psi}_3$, $\tilde{\Psi}_8$ etc. wave functions of the ^5E state is small.

Magnetic Field Splitting

In a magnetic field the perturbation Hamiltonian in Eq. (A1) will also include the term

$$\mathcal{H}=\beta\mathbf{B}\cdot(\mathbf{L}+2\mathbf{S}), \quad \text{(A11)}$$

TABLE VIII. Ten wave functions, their irreducible representations and basis functions for the levels of ^5E. The index i denotes the wave function Ψ_i, F_n is the normalizing factor, and the entries in the table are the contributions to Ψ_i from the various $|M_L M_S\rangle$ functions given in the top row. The levels are arranged in order of increasing energy. Note that $F_n>0$. $u=\sqrt{2}$, $v=\sqrt{3}$, $w=\sqrt{6}$.

i	Irr. rep.	$(F_n)^2$	$\|22\rangle$	$\|21\rangle$	$\|20\rangle$	$\|2\bar{1}\rangle$	$\|2\bar{2}\rangle$	$\|02\rangle$	$\|01\rangle$	$\|00\rangle$	$\|0\bar{1}\rangle$	$\|0\bar{2}\rangle$	$\|\bar{2}2\rangle$	$\|\bar{2}1\rangle$	$\|\bar{2}0\rangle$	$\|\bar{2}\bar{1}\rangle$	$\|\bar{2}\bar{2}\rangle$	Basis
1	Γ_1	8	1				1			2			1				1	xyz
3	Γ_4	4	−1				1						−1				1	$-uS_z$
8	Γ_4	8				1			$+w$							1		S_x+iS_y
14	Γ_4	8		1							$+w$			1				S_x-iS_y
2	Γ_3	8	1				1			−2			1				1	$3z^2-r^2$
21	Γ_3	4			1			1				1			1			$v(x^2-y^2)$
9	Γ_5	8				$+v$			$-u$							$+v$		$-xz-iyz$
15	Γ_5	8		$+v$							$-u$			$+v$				$+xz-iyz$
22	Γ_5	2						1				−1						$iuxy$
20	Γ_2	4			1			−1				−1			1			$S_xS_yS_z$

TABLE IX. Fifteen wave functions, their irreducible representations and basis functions for the levels of $^5T_2$. See caption of Table VIII for the definitions of the symbols.

i	Irr. rep.	$(F_n)^2$	$\|22\rangle$	$\|21\rangle$	$\|20\rangle$	$\|2\bar{1}\rangle$	$\|2\bar{2}\rangle$	$\|12\rangle$	$\|11\rangle$	$\|10\rangle$	$\|1\bar{1}\rangle$	$\|1\bar{2}\rangle$	$\|\bar{1}2\rangle$	$\|\bar{1}1\rangle$	$\|\bar{1}0\rangle$	$\|\bar{1}\bar{1}\rangle$	$\|\bar{1}\bar{2}\rangle$	$\|\bar{2}2\rangle$	$\|\bar{2}1\rangle$	$\|\bar{2}0\rangle$	$\|\bar{2}\bar{1}\rangle$	$\|\bar{2}\bar{2}\rangle$	Basis
10	Γ_5	60				−3				$-w$							6				3		$-xz-iyz$
16	Γ_5	60		3				6							$-w$				−3				$+xz-iyz$
23	Γ_5	20			2				$+w$							$-w$				−2			$iuxy$
4	Γ_4	6	−1				−1				−1			+1				+1				+1	$-uS_z$
11	Γ_4	12				1				$+w$							2				−1		S_x+iS_y
17	Γ_4	12		−1				2							$+w$				1				S_x-iS_y
5	Γ_3	6	+1				−1				−1			−1				−1				+1	$3z^2-r^2$
24	Γ_3	2							1							1							$v(x^2-y^2)$
12	Γ_5	40				2				$-w$							1				−2		$-xz-iyz$
18	Γ_5	40		−2				1				5			$-w$				2				$+xz-iyz$
25	Γ_5	30			3				$-w$							$+w$				−3			$iuxy$
6	Γ_4	12	1				1				−2			2				−1				−1	$-uS_z$
13	Γ_4	24				2				$-w$					−3		1				−2		S_x+iS_y
19	Γ_4	24		−2				1				−3				$-w$			2				S_x-iS_y
7	Γ_1	12	−1				1				−2			−2				1				−1	xyz

where β is the Bohr magnetron and the magnetic induction $\mathbf{B}$ is

$$\mathbf{B}=\mu_0(\mathbf{H}+\mathbf{M}). \tag{A12}$$

Here μ_0 is the permeability of free space and $\mathbf{M}$ the magnetization of the sample. For our CdTe samples $\mathbf{M}\ll\mathbf{H}$ so that we can use $\mathbf{B}=\mu_0\mathbf{H}$. We choose to apply $\mathbf{B}$ along the z axis, i.e., along any of the $\langle 100\rangle$ axes. The matrix of interest is now $\langle\tilde{\Psi}_i|L_z+2S_z|\tilde{\Psi}_j\rangle$, and the $\tilde{\Psi}_i$ are given in Eq. (A10). This magnetic field perturbation puts some diagonal as well as many off-diagonal matrix elements into the original 25×25 matrix. The magnetic field produces interactions among the various levels of ^5E as well as between the ^5E and $^5T_2$ manifolds. A calculation of the magnitude of the ^5E to $^5T_2$ coupling shows that the effect on the energy levels is <0.1 cm^{-1} for magnetic induction values up to 15 T, thus these effects are neglected. The effect of the coupling between the 10 different ^5E levels is given by four matrices, where the matrix elements $d_i{}^j$ are

$$d_i{}^j=\langle\tilde{\Psi}_i|\mathcal{H}_{cf}+\lambda\mathbf{L}\cdot\mathbf{S}+(L_z+2S_z)\beta B_z|\tilde{\Psi}_j\rangle,$$

The four matrices are

$$\begin{array}{c|ccc} i\backslash j & 1 & 2 & 3 \\ 1 & E_1{}^0 & 0 & d_1{}^3 \\ 2 & 0 & E_2{}^0 & d_2{}^3 \\ 3 & d_1{}^3 & d_2{}^3 & E_3{}^0 \end{array} \qquad \begin{array}{c|ccc} i\backslash j & 20 & 21 & 22 \\ 20 & E_{20}{}^0 & 0 & d_{20}{}^{22} \\ 21 & 0 & E_2{}^0 & d_{21}{}^{22} \\ 22 & d_{20}{}^{22} & d_{21}{}^{22} & E_9{}^0 \end{array}$$

$$\begin{array}{c|cc} i\backslash j & 8 & 9 \\ 8 & E_3{}^0+\beta B_z g(\Gamma_4) & d_8{}^9 \\ 9 & d_8{}^9 & E_9{}^0-\beta B_z g(\Gamma_5) \end{array} \qquad \begin{array}{c|cc} i\backslash j & 14 & 15 \\ 14 & E_3{}^0-\beta B_z g(\Gamma_4) & -d_8{}^9 \\ 15 & -d_8{}^9 & E_9{}^0+\beta B_z g(\Gamma_5) \end{array}. \tag{A13}$$

The $g(\Gamma_4)$ and $g(\Gamma_5)$ are the effective gyromagnetic ratios of the Γ_4 and Γ_5 levels. The $E_i{}^0$ are the energies of the various levels in zero magnetic field (see Table V).

TABLE X. Exact values for the c_i coefficients for the $\tilde{\Psi}_i$ eigenfunctions of the ^5E levels of Fe^{2+} in CdTe. Values of $\lambda=-100$ cm^{-1}, $Dq=-248$ cm^{-1} have been used.

Irr. rep.	i	c_i	i	c_i	i	c_i
Γ_1	1	+0.9847	7	−0.1744		
Γ_4	3	+0.9873	4	+0.0988	6	−0.1244
Γ_3	2	+0.9900	5	+0.1412		
Γ_5	9	+0.9947	10	+0.0856	12	−0.0570
Γ_2	20	+1.0000				

All the off-diagonal coefficients go to zero when $B_z=0$. Values for the seven $d_i{}^j$ coefficients can be obtained approximately or exactly as given in Table XI. Note that the exact values show that the approximate relationships $d_1{}^3=d_2{}^3$ and $d_{20}{}^{22}=-d_{21}{}^{22}$ are not strictly true. The matrices in Eq. (A13) have been solved exactly to give the 10 different energy levels as a function of the applied magnetic induction. The results are shown in Fig. 12 for B along any of the three ⟨100⟩ axes. Note that the resultant levels for $B_z>0$ are all singlets. The degeneracies have been completely removed.

Magnetic Susceptibility

The magnetic susceptibility as a function of temperature can be calculated once the energies of the 10 different levels as a function of B are known. The susceptibility is defined as

$$\chi_V=\lim_{H\to 0}\partial M/\partial H, \tag{A14}$$

where $\mathbf{H}$ is the applied magnetic field, $\mathbf{M}$ is the induced dipole moment per unit volume, and V, the subscript of χ, denotes that M is taken per unit volume. In the SI units employed here,

$$\mathbf{B}=\mu_0(\mathbf{H}+\mathbf{M}). \tag{A15}$$

For a multilevel system we need to use the following expression[38] for χ_V:

$$\chi_V=(\mu_0 NkT/V)\lim_{B\to 0}(\partial^2 \ln Z/\partial B^2),$$
$$Z=\sum_i \exp(-E_i/kT), \tag{A16}$$

where N is the total number of Fe^{2+} ions in the sample, V is the sample volume, k is Boltzmann's constant, T is the absolute temperature, Z is the partition function, and E_i is the energy of the ith level and depends on $\mathbf{B}$. The value of χ_V as a function of temperature is given by

$$(\chi_V/\chi_{V0})=\sum_{m=1}^{5} n_m \exp(-e_m x)/\sum_{m=1}^{5} p_m \exp(-e_m x), \tag{A17}$$

where $x=E^0(\Gamma_4)/kT$, χ_{V0} is the value of χ_V at $T=0°K$ and where e_m, n_m, and p_m are given in Table VII. In the perturbation theory limit when $\sigma=0$ the expression of Eq. (A17) reduces to

$$(\chi_V/\chi_{V0})=\frac{(\sinh 2x+\frac{1}{8}x\cosh x+\frac{3}{8}\sinh x)}{(\cosh 2x+3\cosh x+1)}. \tag{A18}$$

The value for χ_V/χ_{V0} given by Eq. (A18) differs from that given by Eq. (A17) by no more than 10% in the temperature range 0 to 300°K. The value of χ_{V0} from perturbation theory is

$$\chi_{V0}=+[16N\mu_0\beta^2(1+4\sigma)^2]/[KV(1-5\sigma)], \tag{A19}$$

where $K=6\lambda^2/\Delta$. The exact calculation is

$$\chi_{V0}=+20.8447N\mu_0\beta^2/VE^0(\Gamma_4). \tag{A20}$$

The molar magnetic susceptibility, χ_M, of Fe^{2+} is just χ_V divided by the number of moles of Fe^{2+} per cubic meter, or

$$\chi_M=\chi_V N_A V/N, \tag{A21}$$

where N_A=Avagadro's number. The calculated value of χ_M versus T is shown in Fig. 13.

TABLE XI. Matrix elements, $d_i{}^j$, for the effect of a ⟨100⟩ magnetic field on the energy levels of the ^5E state of Fe^{2+} in CdTe. β=Bohr magneton=0.92732×10^{-23} J/T, B_z=magnetic induction in T, g=gyromagnetic ratio, and $\sigma=|\lambda|/\Delta=+0.04032$.

Quantity	Approximate value	Exact value
$d_1{}^3/\beta B_z$	$-2\sqrt{2}(1+4\sigma)=-3.2846$	−3.2286
$d_2{}^3/\beta B_z$	$-2\sqrt{2}(1+4\sigma)=-3.2846$	−3.2723
$d_{20}{}^{22}/\beta B_z$	$-2\sqrt{2}=-2.8284$	−2.7993
$d_{21}{}^{22}/\beta B_z$	$+2\sqrt{2}=+2.8284$	+2.8426
$d_8{}^9/\beta B_z$	$-\sqrt{3}(1+2\sigma)=-1.8717$	−1.8348
$g(\Gamma_4)$	$1-2\sigma=+0.9194$	+0.9404
$g(\Gamma_5)$	$1+6\sigma=+1.2419$	+1.3045